A New Technique for Connecting a Dual Excitation Synchronous Generator to the Power Grid

Roberto De Fazio [1] , Ayman Alerksousi [2], Lorenzo Spongano [1] , Bassam Al-Naami [3] , Abdullah Al-Odienat [4] and Paolo Visconti [1,*]

[1] Department of Innovation Engineering, University of Salento, 73100 Lecce, Italy; roberto.defazio@unisalento.it (R.D.F.); lorenzo.spongano@unisalento.it (L.S.)
[2] Department of Electrical Power Engineering, Damascus University, Damascus P.O. Box 30621, Syria; dr.ayman.arksosi@gmail.com
[3] Department of Biomedical Engineering, Faculty of Engineering, The Hashemite University, Zarqa 13133, Jordan; b.naami@hu.edu.jo
[4] Department of Electrical Engineering, Mutah University, Al Karak 61710, Jordan; odienat@mutah.edu.jo
* Correspondence: paolo.visconti@unisalento.it

Abstract: Due to an increasing demand for electric power and changes in the typology of loads, stability has become a major concern in power systems. As the system stability is directly related to the response of the connected generator, recent research has focused on enhancing generators' stability and improving their response to load variations. This study focuses on adding another excitation winding on to the *q*-axis, perpendicular to the conventional excitation winding on the *d*-axis, to control both active and reactive power. This paper studies and compares the performance of the dual excitation synchronous generator (DESG) to conventional synchronous generators. The mathematical equations are derived, and a mathematical model is then developed. The experimental tests have been conducted using a laboratory model consisting of a two-phase synchronous generator driven by a DC motor with different loads. The obtained results and radial diagrams for the different loading types are presented and evaluated. Therefore, a new approach has been designed to connect the DESG directly to the power grid without any electronic components using a special coupling that works in one direction. Two perpendicular excitation coils, *d* and *q*, were formed from the existing coils, and the tests were carried out on all loads, ensuring that the revolving angle (i.e., the stability angle φ) was fixed. The results show that the proposed method offers significant cost savings, potentially amounting to 15–20% of the unit price. The experimental results confirm that the DESG significantly improves the generator stability by maintaining a constant rotor angle δ, which requires using an automatic angle regulator (AAR) in addition to the conventional automatic voltage regulator (AVR).

Keywords: dual excitation synchronous generator; DESG mathematical model; DESG characteristics; DESG two-axis flux linkage equations

1. Introduction

A dual excitation synchronous generator (DESG) is a type of synchronous generator with two separate excitation sources. One excitation source is used to create a magnetic field in the stator, and the other is used to create a magnetic field in the rotor. This allows the generator to operate at a variable speed, which is useful for applications such as wind turbines and hydroelectric power plants [1]. The DESG has several advantages over traditional synchronous generators, including the ability to operate at a variable speed, which means that it can better match the varying speed of the input power source (such as wind or water). This can result in higher efficiency and a more stable output voltage [2–4]. Another advantage of the DESG is that it can provide reactive power support to the power grid. Reactive power is needed to maintain voltage levels and stabilize the grid, and

synchronous generators are often used to provide this support. With the DESG, both the stator and rotor can be used to provide reactive power, which can help to reduce the need for additional equipment such as capacitors [3]. The DESG has been recognized in the literature as a valuable approach to enhancing both steady-state and dynamic stability, improving system reliability, and enabling independent control of the active and reactive power [5–8]. Additionally, it has been revealed that the frequency regulation and the control of generator terminal voltage magnitude can be achieved by manipulating specific parameters of the excitation currents [9].

In the literature, many authors have addressed DESGs from different perspectives. In [9], a comprehensive analysis is presented, which offers an accurate representation of the machine. A per-unit system is utilized to avoid errors caused by the conventional system when considering saliency. The external connection is examined in a generalized form, enabling the study of the machine performance when connected to an infinite bus through a general transmission system. A small displacement model is also derived and organized in a suitable format for investigating dynamic stability issues. This model is a valuable tool for examining the impact of various excitation regulation schemes on the machine's dynamic behavior [10,11].

Different strategies have been used for controlling the electrical power generation of a DESG as a generation system for wind energy conversion. In Ref. [4], H. M. Yassim et al. presented a control technique for maximizing the power conversion efficiency and regulating the reactive power injected into the grid for a DESG operating as a constant-speed constant-frequency (CSCF) generation system. This method is based on managing the field-current space phasor magnitude and the field-voltage phase angle in order to control the active and reactive power provided by the DESG. Furthermore, in Ref. [12], the same authors developed a method for controlling the low voltage ride through (LVRT) capability in DESGs, acting on the field-voltage space phase, and exploiting the added reactive power to promote grid voltage recuperation under grid faults. The proposed strategy was validated through experimental tests and simulations for a 1.1 kW DESG wind turbine. Similarly, in Ref. [13], the authors proposed a novel strategy to control the reactive power in DESGs operating in CSCF modality and a variable-speed constant-frequency (VSCF) generating system, improving the conversion efficiency and reducing the copper losses. This strategy is founded on regulating the magnitude and phase angle of the field winding to control the active and reactive power, respectively. The simulation results validated the proposed control strategy using a 1.1 kW DESG. In addition, S. D'Arco et al. in Ref. [14] introduced a control strategy for DESG operation applied to variable-speed wind turbines, enabling them to be actively controlled [14]. This strategy maximizes the generated active power, keeping the active power in the rotor stable to a reference value. Doubly fed induction generators (DFIG) are commonly used as alternatives to DESGs for wind energy conversion systems, and these power generation systems require accurate control strategies for optimizing the power they produce. In Ref. [15], Z. Dekali et al. proposed an indirect power control strategy for the machine side converter (MSC), setting the current target values to obtain the desired active and reactive power injected into the grid. The strategy implemented a field-oriented control (FOC) of the *dq* frame to regulate the stator power by acting on the rotor current components.

Compared to methodologies proposed in the published and previously analyzed scientific works, the proposed direct connection technique is computationally simpler, enabling the direct connection of the DESG to the grid without the need for any power components or converters [1–5]. Therefore, the proposed technique does not require an electronic power converter to adapt the produced power to be injected into the grid under variable speed conditions, unlike other solutions reported in the scientific literature [4,5]. Moreover, by removing the need for an electronic power converter, the reliability of the wind generating system is significantly improved. The proposed strategy keeps the rotor angle stable regardless of the injected power by controlling the signals applied to the cross-sectional coils, thus regulating the stability angle (ϕ). In addition, the proposed solution

allows the control of active and reactive power independently, thus enabling the regulation of the power factor.

In summary, this research article focuses on the performance evaluation of DESGs compared to conventional synchronous generators. The mathematical equations are derived, and a mathematical model has been developed. The paper also presents a new mechanical coupling method for directly connecting the wind turbine with the synchronous generator to the network without any electronic components. The study uses two laboratory models: In the first one, a DESG with a 2 kW capacity is driven by a DC motor representing the wind turbine. In this model, the two machines are linked through the developed mechanical coupling proposed in the research article. The second model is a three-phase laboratory machine with a nominal capacity of 2.3 KVA. Two perpendicular excitation coils, *d* and *q*, were formed from the existing coils, and the tests were carried out on different loads, ensuring that the torque angle was fixed. The proposed mechanical coupling method enables the generator to be directly connected to the electric network without needing any electronic components. The obtained results demonstrate that the developed DESG-based solution outperforms the conventional generator in many aspects, including a simplification from the point of view of the elements necessary for connection to the grid, and therefore provides a significant cost saving. The only limitation of the proposed technique is the need for an automatic control system to regulate the signals on the quadrature coils and manage the power injection into the power grid.

2. The DESG Mathematical Model

By applying the voltage U_{ed} on the direct winding of W_{ed} turns, a current I_{ed} is drawn, forming the magnetomotive force (MMF) F_{ed} given by the following equation [11,16]:

$$F_{ed} = \frac{I_{ed} \, W_{ed}}{2P} \, \text{A.T/Pole} \tag{1}$$

Furthermore, by applying the voltage U_{eq} on the direct winding of W_{eq} turns, a current I_{eq} is drawn, forming a magnetomotive force (MMF) F_{eq}, as follows:

$$F_{eq} = \frac{I_{eq} \, W_{eq}}{2P} \text{A.T/Pole} \tag{2}$$

If $W_{eq} = W_{ed}$ and $U_{ed} = U_{eq}$, then the following equality is obtained: $F_{eq} = F_{ed}$ (Figure 1). As shown in Figure 1, if $W_{eq} \neq W_{ed}$, then it turns out $F_{eq} = (0.2 \div 0.3) \, F_{ed}$.

Figure 2 shows the space distribution of the excitation windings and magnetic flux of both types of synchronous generators. The main operation principle for any generator is based on the interaction between the magnetic fields. So, F_{ed} and F_{eq} generate the magnetic fluxes φ_{ed} and φ_{eq}, respectively, and when the rotor rotates at a speed n_1 (RPM), each of these fluxes will rotate at the same speed and generate the electromotive forces (EMF) in each phase of the armature E_{od} and E_{oq} [17–19]. Figure 3 shows the vector diagrams of both conventional and dual machines, where:

θ represents the load angle between the voltage U and E.
φ represents the angle between E_0 and the *q*-axis, indicated in the text as the stability angle.
A represents the power factor of the load.
ψ represents the angle between the current I_a and the *q*-axis ($\theta = \delta \pm \psi$, $\psi = \alpha + \delta$).
δ represents the shift angle between U and E_0 (displacement of the rotors and the *q*-axis), indicated in the text as the rotor angle.
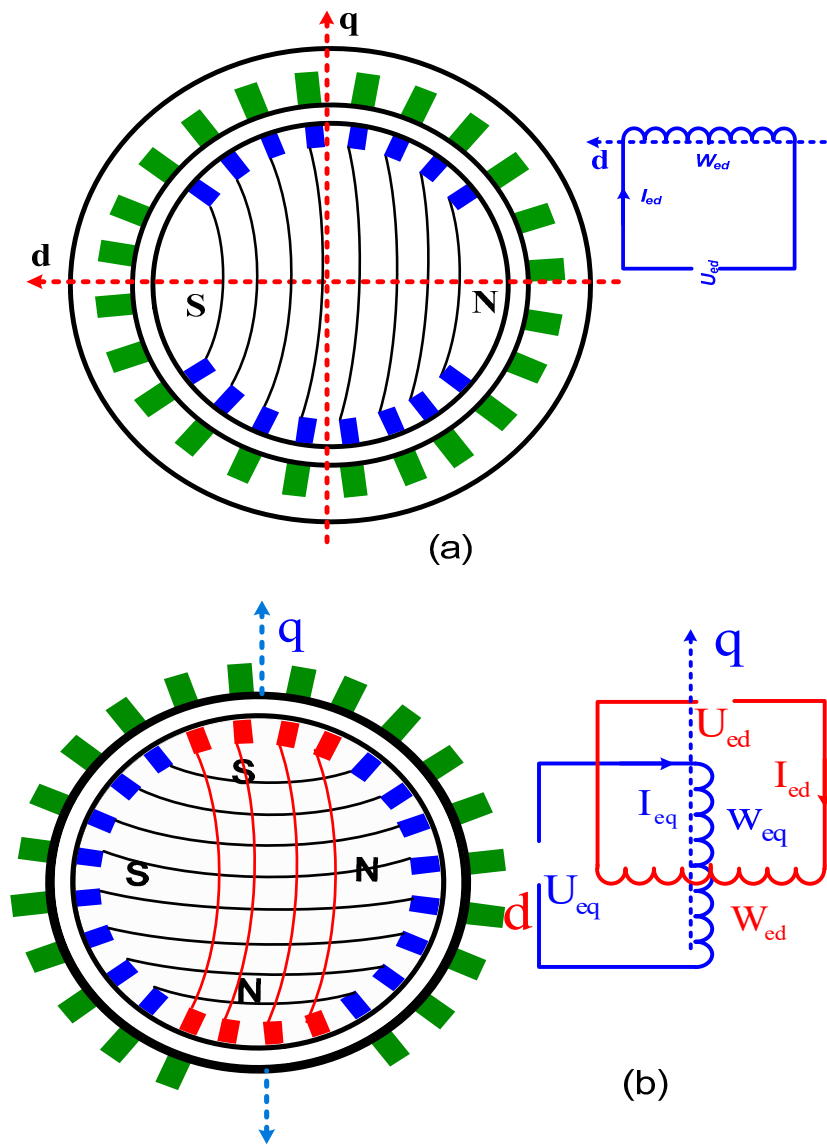
Figure 1. The magnetic flux linkage for (**a**) conventional synchronous generator, and (**b**) DESG.
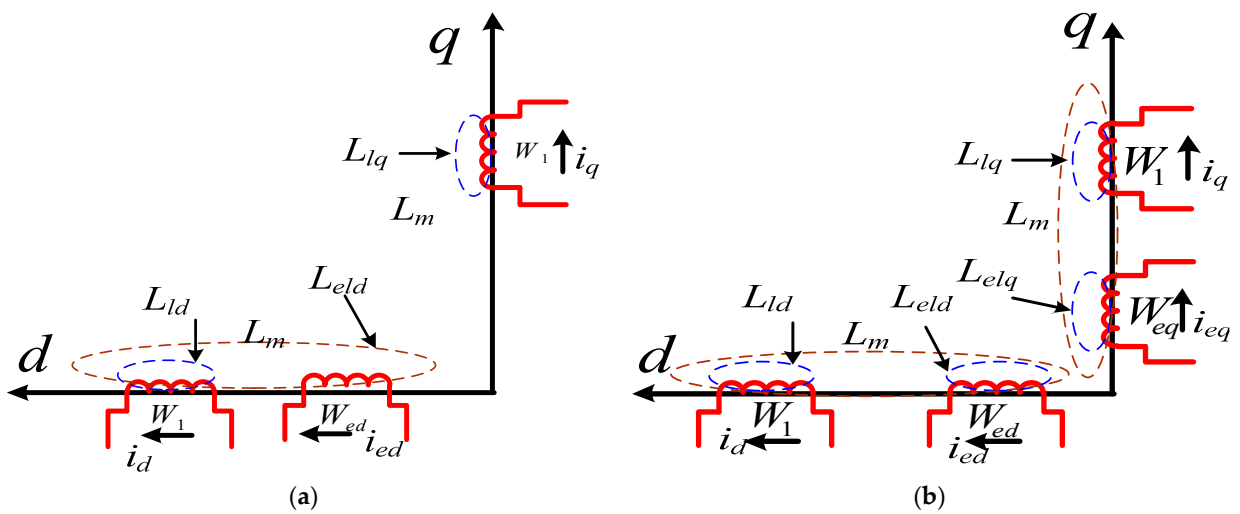
Figure 2. The space distribution of the excitation coils and magnetic flux for the conventional synchronous generator (**a**) and the dual excitation synchronous generator (DESG) (**b**).

Figure 3. (**a**) Vector diagram of the conventional generator and (**b**) of the dual excitation synchronous generator (DESG).

In a conventional machine, the equality δ = θ is achieved, while in a DESG, the rotor angle δ differs from the load angle θ because the excitation is taken on the two axes. It could be zero if (θ = φ), which means more ability to handle the load variations and higher margins of stability [20,21].

Figure 4 shows the vector diagram of the DESG [22]. The active (*P*) and reactive (*Q*) power delivered by the generator can be stated as follows (Equations (3) and (4)) [22,23]. Figure 5 shows the P and Q variations as a function of δ keeping U, E_{oq}, and E_{od} constant.

Figure 4. The vector diagram for a DESG with the effect of the armature reaction.

Figure 5. Variations of Q and P as a function of the load (θ) and rotor (δ) angles: Q trend (**a**) and P trend (**b**).

Equations (3) and (4) explain that a small increase in δ has no effect on the active power component P_d on the *d*-axis. In contrast, the component P_q on the *q*-axis would differ greatly, and the system's power factor will be improved consequently [24].
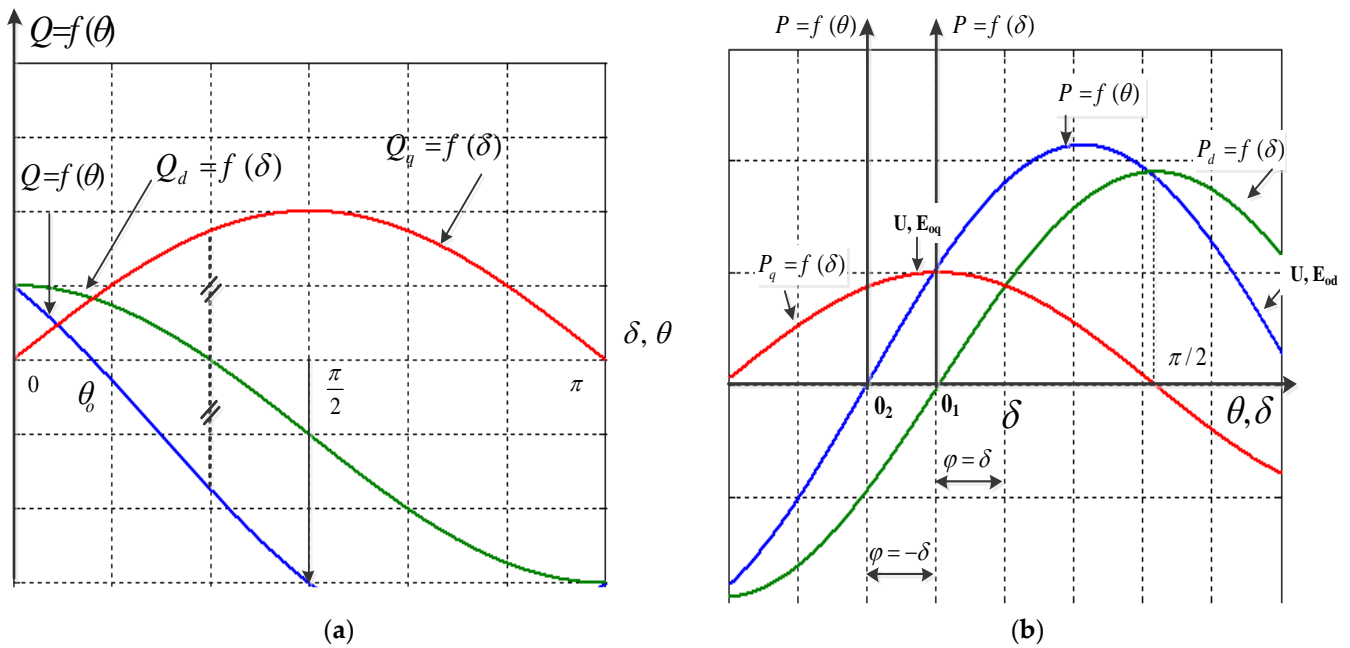
$$P = \frac{mUE_0}{X_d}\sin\theta = \frac{mUE_0}{X_d}\sin(\delta + \varphi) = \frac{mUE_{od}}{X_s}\sin\delta + \frac{mUE_{od}}{X_s}\cos\delta = P_d + P_q \quad (3)$$

$$\begin{aligned} Q &= \frac{mUE_0}{X_S}\cos\theta - \frac{mU^2}{X_s} = \frac{mUE_0}{X_s}\cos(\delta + \varphi) - \frac{mU^2}{X_s} \\ &= \frac{mUE_{od}}{X_s}\cos\delta - \frac{mU^2}{X_s} - \frac{mUE_{oq}}{X_s}\sin\delta = Q_d - Q_q \end{aligned} \quad (4)$$

$$\tan\alpha = \frac{Q_d - Q_q}{P_d + P_q}$$

The rotor angle stability is the capability of interconnected synchronous power generators operating in the power system to remain in synchronized conditions. During normal generator operation, the rotor magnetic field and that of the stator rotate at the same speed. However, an angular shift between the magnetic field of the rotor and stator will be present, depending on the electrical torque (power) delivered by the generator. An increase in the generator speed (i.e., the wind turbine) will cause the rotor angle to advance to a new position relative to the rotating stator's magnetic field. On the other hand, mechanical torque reduction causes a drop in the rotor angle with respect to the stator field. In equilibrium conditions, there will be a balance between the input mechanical torque and output electrical torque of each electrical machine (generator), and their speed will remain the same. If the balance is upset, the result is acceleration or deceleration of the machines' rotors; if an interconnected generator moves faster, its rotor angle will advance compared to that of the slower machine. This results in an increase in the load delivered by the faster generator and a decrease in the load delivered by the slow one. In this case, the speed difference between the two generators reduces, as well as the angular shift. Instead, beyond a certain point, if the angular shift increases further, there will be a decrease in power transfer by the fast machine. A subsequent further increase in angular separation between the two generators may lead to unstable operation due to the lack of synchronization between the generators.

It is well known that the condition of stability for the conventional generator is:

1- Without excitation regulation:

$$Q + \frac{U^2}{X_s} > 0 \tag{5}$$

2- With excitation regulation:

$$Q + \frac{U^2}{X_s} + \frac{\alpha_d}{X_s \sqrt{\left[P^2 + \left(Q^2 + \frac{U^2}{X_s} \right)^2 \right]}} \, U.P > 0 \tag{6}$$

where $\alpha_d = \Delta e_{od} / \Delta\theta$ is the excitation voltage variation coefficient with respect to θ. From these equations, when $P \neq 0$, by increasing α_d, the stability margin will expand. When P decreases, the validity of the excitation regulation will decrease and approach the inefficient regulation level, which is considered the main disadvantage of conventional generators [25–27].

On the other hand, the condition of stability for the DESG is:

1- Without excitation regulation:

$$Q + \frac{U^2}{X_s} > 0 \tag{7}$$

2- With excitation regulation:

$$Q + \frac{U^2}{X_s} + \frac{U}{X_s} \left(\alpha_d \sin\delta + \alpha_q \cos\delta \right) > 0 \tag{8}$$

This result means that there are no limits to the output power stability, and the stability is independent of δ [28,29]. Practically, it is found that the reactive capacitive power would be increased two to three times more than in the case of conventional generators, which enhances the stability of the DESG. Another advantage of a DESG is its ability to work at asynchronous speed ($n \neq n_1$) for a long time, even with a large load; this operation mode is called an asynchronous generator.

3. The Self and Mutual Inductances of the DESG

The DESG consists of a set of seven coils (3ph + 2k + 2f), and there are seven corresponding voltage equations, in which many of the coefficients are periodic functions of the angle β, as shown in Figure 6 [10].

The self-inductances L_{KKq}, L_{KKd}, L_{ffq}, and L_{ffd} of the two fields, the two damper coils, and the mutual inductances L_{fqkq} and L_{fdkd} between F_d and K_d, and F_q and K_q, respectively, are all constant. The armature self-inductances L_{cc}, L_{bb}, and L_{aa} vary periodically between a maximum value when the coil is on the pole axis and a minimum value when it is on the interpolar axis. The following equations report the exact relationships between the terms discussed above.

$$\begin{cases} L_{aa} = A_0 + A_2\cos 2\beta + A_4\cos 4\beta + \ldots + \\ L_{bb} = A_0 + A_2\cos 2(\beta - 2\pi/3) + A_4\cos 4(\beta - 2\pi/3) + \ldots + \\ L_{bb} = A_0 + A_2\cos 2(\beta - 4\pi/3) + A_4\cos 4(\beta - 4\pi/3) + \ldots + \end{cases} \tag{9}$$

The armature mutual inductances L_{ca}, L_{bc}, and L_{ab} also vary periodically and are given by the same expressions with β replaced by $(\beta - 2\pi/3)$ and $(\beta - 4\pi/3)$, respectively:

$$\begin{cases} L_{bc} = -B_0 + B_2\cos 2\beta + B_4\cos 4\beta + \ldots + \\ L_{ca} = -B_0 + B_2\cos 2\left(\beta - \frac{2\pi}{3} \right) + B_4\cos 4\left(\beta - \frac{2\pi}{3} \right) + \ldots + \\ L_{ab} = -B_0 + B_2\cos 2\left(\beta - \frac{4\pi}{3} \right) + B_4\cos 4\left(\beta - \frac{4\pi}{3} \right) + \ldots + \end{cases} \tag{10}$$
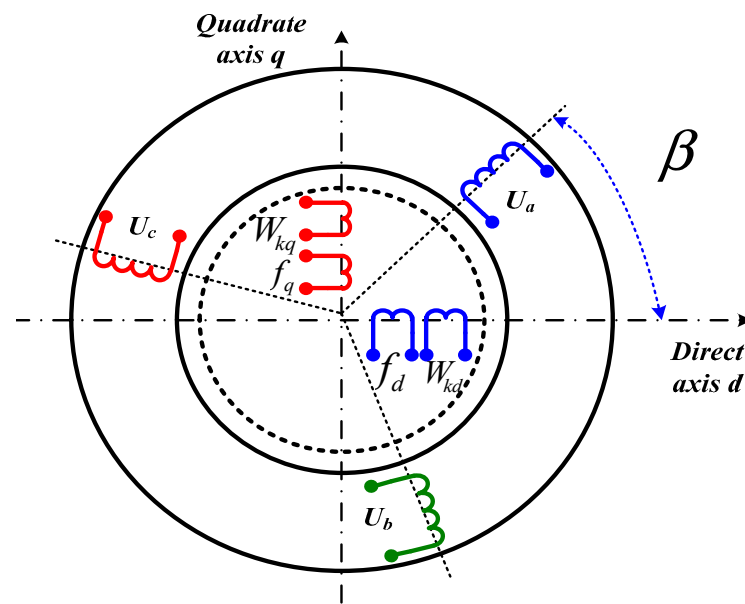
Figure 6. The synchronous machine with two excitation coils and two damper coils.

The mutual inductance between an armature coil and a field or damper coil L_{afd} varies periodically with a period of (2π). L_{afd} is at maximum when the phase A is on the direct axis and zero when the phase A is on the quadrature axis, thus:

$$\left\{\begin{array}{l} L_{afd} = C_1\cos\beta + C_3\cos 3\beta + \ldots + \\ L_{afq} = C_1\sin\beta - C_3\sin 3\beta + \ldots + \\ L_{akd} = D_1\cos\beta + D_3\cos 3\beta + \ldots + \\ L_{akq} = D_1\sin\beta - D_3\sin 3\beta + \ldots + \end{array}\right\} \tag{11}$$

The remaining inductances involving (B) (namely L_{bfd}, L_{bfq}, L_{bkd}, and L_{bkq}) are obtained by replacing β with ($\beta - 2\pi/3$), and those concerning C (namely L_{cfd}, L_{cfq}, L_{ckd}, and L_{ckq}) are obtained by replacing β with ($\beta - 4\pi/3$) in the appropriate expressions [10].

For many purposes, the equations can be simplified by neglecting the third-order Fourier terms and the higher ones. The equations relating the terminal voltages to the currents in the seven circuits of Figure 6 are based on the coefficients reported in the following tables (Tables 1 and 2). The mutual and self-inductances of the DESG are represented in Figures 7 and 8, respectively.

Table 1. Summary table of the different inductances for the coils of Figure 6.

	a	b	c	f_d	f_q	k_d	K_q
a	L_{aa}	L_{ab}	L_{ac}	L_{afd}	L_{afq}	L_{akd}	L_{akq}
b	L_{ba}	L_{bb}	L_{bc}	L_{bfd}	L_{bfq}	L_{bkd}	L_{bkq}
c	L_{ca}	L_{cb}	L_{cc}	L_{cfd}	L_{cfq}	L_{ckd}	L_{ckq}
f_d	L_{afd}	L_{bfd}	L_{cfd}	L_{fdfd}	L_{fdfq}	L_{fdkd}	L_{fdkq}
f_q	L_{afq}	L_{bfq}	L_{cfq}	L_{fqfd}	L_{fqfq}	L_{fqkd}	L_{fqkq}
k_d	L_{akd}	L_{bkd}	L_{ckd}	L_{kdfd}	L_{kdfq}	L_{kdkd}	L_{kdkq}
k_q	L_{akq}	L_{bkq}	L_{ckq}	L_{kqfd}	L_{kqfq}	L_{kqkd}	L_{kqkq}

Table 2. Expressions derived for the different inductances for the coils of Figure 6.

|	a	b	C	f_d	f_q	k_d	K_q
a	$= R_a + L_{1s} + L_0 - L_{ms}\cos 2\beta$	$= -\frac{1}{2}L_0 - L_{ms}\cos 2(\beta - \frac{\pi}{3})$	$= -\frac{1}{2}L_0 - \cos 2(\beta + \frac{\pi}{3})$	L_{afd}	L_{afq}	L_{akd}	L_{akq}
b	$= -\frac{1}{2}L_0 L_{ms}\cos 2(\beta - \frac{\pi}{3})$	$= R_a + L_{1s} + L_0 = -L_{ms}\cos 2(\beta - \frac{2\pi}{3})$	$= -\frac{1}{2}L_0 - L_{ms}\cos 2(\beta - \pi)$	L_{bfd}	L_{bfq}	L_{bkd}	L_{bkq}
c	$= -\frac{1}{2}L_0 - \cos 2(\beta + \frac{2\pi}{3})$	$= -\frac{1}{2}L_0 - \cos 2(\beta + \frac{\pi}{3})$	$= R_a + L_{1s} + L_0 - L_{ms}\cos 2(\beta + \frac{2\pi}{3})$	L_{cfd}	L_{cfq}	L_{cfq}	L_{ckd}
f_d	$L_{afd} = L_{afd}\cos 2(\beta + \frac{2\pi}{3})$	$L_{bfd} = L_{bfd}\cos 2(\beta - \frac{2\pi}{3})$	$L_{cfd} = L_{cfd}\cos 2(\beta + \frac{2\pi}{3})$	$R_{fd} + L_{fdfd}$	0	L_{fdkd}	0
f_q	$L_{afq} = L_{afq}\sin \beta$	$L_{bfq} = L_{bfq}\sin 2(\beta - \frac{2\pi}{3})$	$L_{cfq} = L_{cfq}\sin 2(\beta + \frac{2\pi}{3})$	0	$R_{fq} + L_{fqfq}$	0	L_{fqkq}
k_d	$L_{akd} = L_{akd}\cos \beta$	$L_{bkd} = L_{bkd}\cos(\beta - \frac{2\pi}{3})$	$L_{ckd} = L_{ckd}\cos(\beta + \frac{2\pi}{3})$	L_{kfdd}	0	$R_{kd} + L_{kdkd}$	0
kq	$L_{akq} = L_{akq}\sin \beta$	$L_{bkq} = L_{bkq}\sin(\beta - \frac{2\pi}{3})$	$L_{ckq} = L_{ckq}\sin(\beta + \frac{2\pi}{3})$	0	L_{kfqq}	0	$R_{kq} + L_{kqkq}$
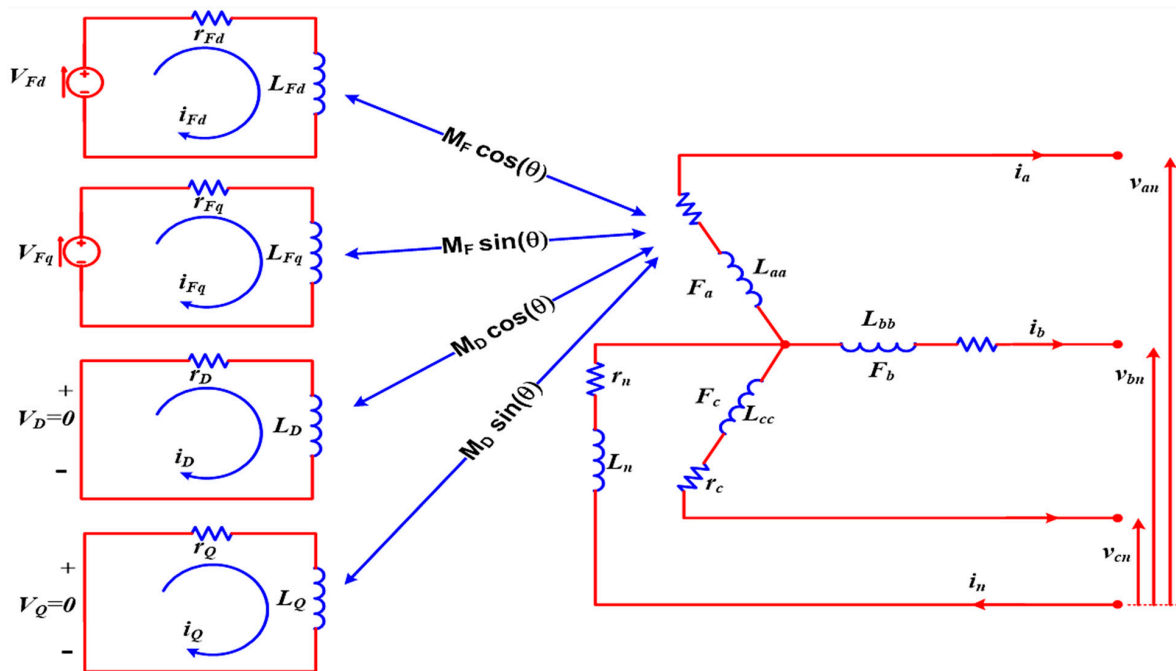
Figure 7. The synchronous machine equivalent circuit: the mutual and self-inductances.
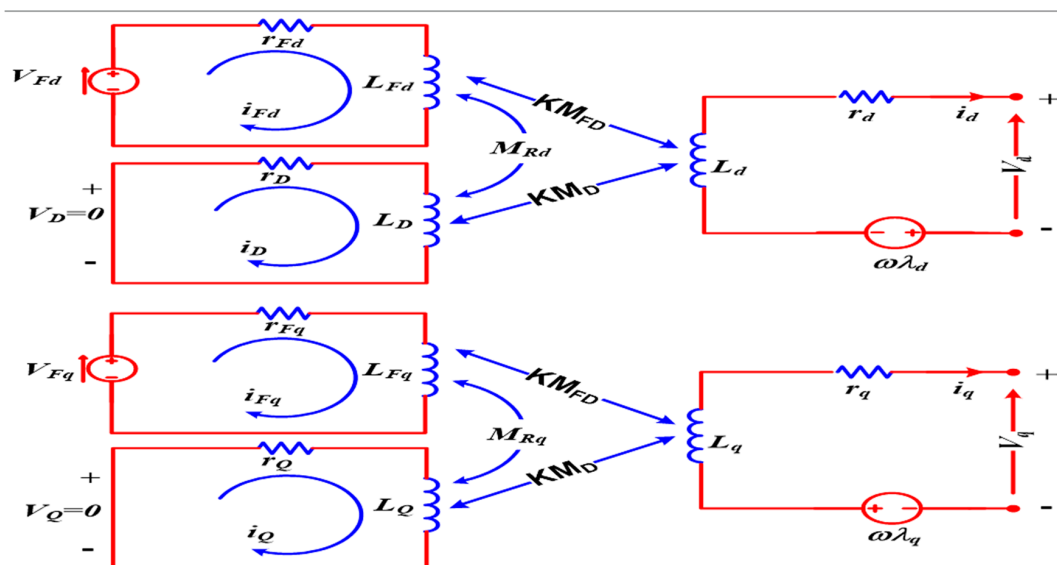

Figure 8. The synchronous machine equivalent circuit: d-q self and mutual inductances.

4. Direct Derivation of the Two-Axis Flux Linkage Equations

The flux linkage, used as a measure of the flux, may be resolved into direct and quadrature axes as (ψ_{md}, ψ_{mq}). The induced voltage in coil A depends on its angular position β and the flux linkage components. The voltage induced by (ψ_{md}) is $-p(\psi_{md} \cos\theta + \psi_{mq} \sin\theta)$. Hence, the total internal voltage, opposing the voltage induced by the main air-gap flux, is $-p(\psi_{md} \cos\theta + \psi_{mq} \sin\theta)$. The current i_a produces a leakage reactance drop $L_1 p i_a$, where L_1 is the leakage inductance of the coil A. i_b and i_c produce the voltage drops $L_m p i_b$ and $L_m p i_c$ across the coil A. L_m is the part of the mutual inductance between the two armatures due to the flux, which does not cross the air gap; note that L_m and L_1 are independent of the rotor position.

The impressed voltage U ᵃ is equal to the sum of the internal voltage due to the main air gap flux, the drops due to the local armature fluxes, and the resistance drop $i_a R_a$. Hence, the related equation is as follows [20]:

$$
\begin{aligned}
u_a \ &= p\left(\psi_{md}\cos\beta + \psi_{mq}\sin\beta\right) + \left(R_a + L_1 p\right)i_a - L_m p i_b - L_m p i_c \\
&= p\left(\psi_{md}\cos\beta + \psi_{mq}\sin\beta\right) + \left(L_1 + L_m\right)i_a - L_m p i_a - L_m p i_b - L_m p i_c + R_a i_a \\
&= p\left(\psi_{md}\cos\beta + \psi_{mq}\sin\beta\right) + \left(L_1 + L_m\right)\left(i_d\cos\beta + i_q\sin\beta + i_s\right) + 3L_m p i_s + R_a i_a \\
&= p\left[\left(\psi_{md} + L_a i_d\right)\cos\beta + \left(\psi_{mq} + L_a i_q\right)\sin\beta\right] + L_s p i_s + R_a i_a
\end{aligned}
\tag{12}
$$

$$
L_a = (L_1 + L_m),\ L_s = L_a - 3L_m,\ \psi_d = \psi_{md} + L_a i_d,\ \psi_q = \psi_{mq} + L_a i_q
\tag{13}
$$
$$
u_a = p\left[\psi_d\cos\beta + \psi_q\sin\beta\right] + L_s p i_s + R_a i_a
$$

4.1. Direct Axis and Quadrature Axis Equations

The equation for a system of stationary mutually-coupled coils comprising the coils *D*, F_d, $D_1 \ldots$, and D_m on the direct axis and the *Q*, F_q, Q_1, $\ldots$, Q_m coils on the quadrature axis can be written in terms of their self and mutual inductances.

The flux linkage (ψ_d) depends only on the direct axis current and is given by:

$$
\psi_d = L_{fdd} i_{fd} + L_{d_1 d} i_{d_1} + L_{d_2 d} i_{d_2} + L_d i_d + L_{d_m d} i_{d_m}
\tag{14}
$$

where $L_{d_m d}$, $L_{d_2 d}$, $L_{d_1 d}$, and L_{fdd} are the mutual inductances between the coils F_d and *D*. L_d is the complete self-inductance of coil D.

The voltage equations for the field and direct axis damper are determined below. The field excitation voltage of D can be calculated as follows:

$$
U_{fd} = \left(R_{fd} + L_{ffd} p\right) i_{fd} + L_{fdd1} p\, i_{d1} + L_{fdd2} p\, i_{d2} + L_{fddm} p\, i_{dm} + L_{fdd} p\, i_d
\tag{15}
$$

The coil voltage of D_1 and D_2 are determined below by the Equations (16) and (17), respectively.

$$
0 = L_{fdd1} p\, i_{fd} + \left(R_{d1} + L_{d1} p\right) i_{d1} + \left(R_{d1d2} + L_{d1d2} p\right) i_{d2} + L_{d1d} p\, i_d
\tag{16}
$$

$$
0 = L_{fdd2} p\, i_{fd} + \left(R_{d1d2} + L_{d1d2} p\right) i_{d1} + \left(R_{d2} + L_{d2} p\right) i_{d2} + \ldots + L_{d2d} p\, i_d
\tag{17}
$$

where L_{d1}, L_{d2}, and L_{ffd} represent the self-inductance of coils D_2, D_1, and F_d with the damper coils. Figure 9 shows the coils of the two-axis synchronous machine. In many cases, u_{fd}, ψ_d, i_d may be eliminated by taking the Laplace transform. The relationship between the Laplace transforms of u_{fd}, ψ_d, and i_d takes the following form:

$$
\psi_d = \frac{Xd(p)}{\omega_0} i_d + \frac{G(p)}{\omega_0} u_{fd}
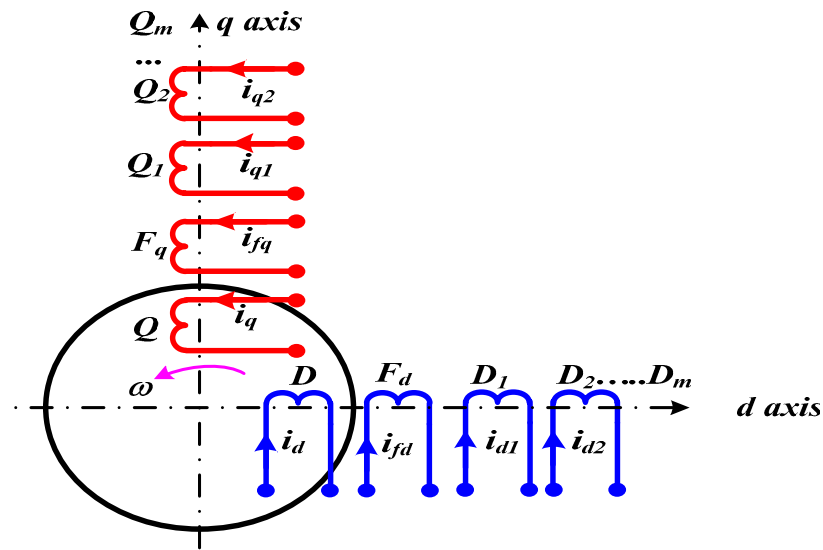\tag{18}
$$

Figure 9. Coils of the two-axis synchronous machine.

The quadrature axis equations in the DESG are similar to those for the direct axis because of the quadrature field winding, and ψ_q depends on the quadrature axis currents [10]:

$$\psi_q = L_{ffq}i_{fq} + L_{q_1q}i_{q_1} + L_{q_2q}i_{q_2} + L_{q_mq}i_{q_m} + L_q i_q \tag{19}$$

where L_{q2q}, L_{q1q}, L_{fqq}, and L_{q_mq} are the mutual inductances of the coils Q_2, Q_1, F_q, and Q (damper coils), respectively, and L_q represents the self-inductance of coil Q. The voltage of the field excitation Q is calculated as follows (Equation (20)):

$$U_{fq} = \left(R_{fq} + L_{ffq}p\right)i_{fq} + L_{fqq1}p i_{q1} + L_{fqq2}p\, i_{q2} + L_{fqqm}p i_{qm} + L_{fqq}p\, i_q \tag{20}$$

Instead, the voltage of the coil Q_1 is determined through the following equations:

$$0 = L_{fqq1}p i_q + \left(R_{q1} + L_{q1}p\right)i_{q1} + \left(R_{q1q2} + L_{q1q2}p\right)i_{q2} + \ldots + L_{q1q}p\, i_q \tag{21}$$

$$0 = \left(R_{q1q2} + L_{q1q2}\, p\right)i_{q1} + \left(R_{q2} + L_{q2}p\right)i_{q2} + \ldots + L_{q2q}p i_q \tag{22}$$

4.2. Simplified Equations of the DESG with Two Field Coils and Two Damper Coils

For most DESGs, the equations used are those of the machine with one field coil F_d, and a damper coil K_D on the direct axis, and one field coil Fq and a damper coil K_Q on the quadrature axis. Therefore, the Equation (11) and related coefficients reported in Tables 1 and 2 can be reduced to the three direct axis equations as reported below:

$$\psi_d = L_{fdd}\, i_{fd} + L_{dkd}i_{kd} + L_d\, i_d \tag{23}$$

$$u_{fd} = (R_{fd} + L_{ffd}p)i_{fd} + L_{fdkd}p i_{kd} + L_{fdd}p i_d \tag{24}$$

$$0 = L_{fdkd}i_{fd} + (R_{kd} + L_{kkd}\, p)\, i_{kd} + L_{dkd}p\, i_d \tag{25}$$

In the quadrature axis, the Equations (19)–(21) can be reduced to three quadrature axis equations, as follows:

$$\psi_q = L_{fqq}i_{fq} + L_{qkq}i_{kq} + L_q i_q \tag{26}$$

$$U_{fq} = \left(R_{fq} + L_{ffq}p\right)i_{fq} + L_{fqkq}p\, i_{kq} + L_{fqq}p\, i_q \tag{27}$$

$$0 = L_{fqkq}p\, i_{fq} + (R_{kq} + L_{kkq}\, p)\, i_{kq} + L_{qkq}p i_q \tag{28}$$

5. Equations of the DESG Using Per-Unit Leakage Inductance

The equations from (20) to (25) become easier to handle when the quantities are transformed on a per-unit basis. In addition, it is assumed that the three per-unit mutual inductances on the direct axis are also equal, and the quadrature axis is equal. So we assume that:

$$L_{fdd} = L_{fdkd} = L_{dkd} = L_{md}, \text{ and } L_{fqq} = L_{fqkq} = L_{qkq} = L_{mq} \tag{29}$$

L_{md} and L_{mq} represent the per-unit mutual inductances, and L_L is the armature leakage inductance. The self-inductance of each coil is the sum of the mutual inductance and the leakage inductance:

$$\left\{ \begin{array}{l} L_d = L_{ld} + L_{md}, L_q = L_{lq} + L_{mq} \\ L_{ffd} = L_{lfd} + L_{md}, L_{ffq} = L_{lfq} + L_{mq} \\ L_{kkd} = L_{lkd} + L_{md}, L_{kkq} = L_{lkq} + L_{mq} \end{array} \right\} \tag{30}$$

Practically, the voltages U_{kd} and U_{kq} are almost equal to zero.

$$\psi_d = (L_{md} + L_{ld})\, i_d + L_{md}i_{fd} + L_{md}i_{kd} \tag{31}$$

$$u_{fd} = L_{md}pi_d + [R_{fd} + (L_{md} + L_{lfd})p]\, i_{fd} + L_{md}pi_{kd} \tag{32}$$

$$0 = L_{md}pi_d + L_{md}pi_{fd} + [R_{kd} + (L_{md} + L_{lkd})p]\, i_{kd} \tag{33}$$

$$\psi_q = \left(L_{mq} + L_{lq}\right) i_q + L_{mq}i_{fq} + L_{mq}i_{kq} \tag{34}$$

$$u_{fq} = L_{mq}pi_q + \left[R_{fq} + \left(L_{mq} + L_{lfq}\right)p\right] i_{fq} + L_{mq}pi_{kq} \tag{35}$$

$$0 = L_{mq}pi_q + L_{mq}pi_{fq} + [R_{kq} + (L_{mq} + L_{lkq})p]\, i_{kq} \tag{36}$$

The basic machine's constants are specified below:

- R_a: armature resistance.
- R_{fd}: direct axis field resistance.
- R_{kd}: direct axis damper resistance.
- R_{fq}: quadrature axis field resistance.
- R_{kq}: quadrature axis damper resistance.
- $X_{md} = \omega_0 L_{md}$: direct axis magnetizing reactance.
- $X_{mq} = \omega_0 L_{mq}$: quadrature axis magnetizing reactance.

The DESG equivalent circuits are given in Figure 10, while the equations related to the six voltages are presented below (Equation (37)).

$$\left\{ \begin{array}{l} U_d = R_a i_d + (L_{md} + L_a)\frac{di_d}{dt} + L_{md}\frac{di_{ed}}{dt} + L_{md}\frac{di_{kd}}{dt} \\ \qquad + (L_{mq} + L_a)\,\omega\, i_q + L_{mq}\,\omega\, i_{eq} + L_{mq}\,\omega\, i_{kq} \\ U_q = -(L_{md} + L_a)\,\omega\, i_d - L_{md}\,\omega\, i_{ed} - L_{md}\,\omega\, i_{kd} + R_a i_q \\ \qquad + (L_{mq} + L_a)\frac{di_q}{dt} + L_{mq}\frac{di_{eq}}{dt} + L_{mq}\frac{di_{kq}}{dt} \\ U_{ed} = L_{md}\frac{di_d}{dt} + R_f i_{ed} + (L_{md} + L_f)\frac{di_{ed}}{dt} + L_{md}\frac{di_{kd}}{dt} \\ U_{eq} = L_{mq}\frac{di_q}{dt} + R_f i_{eq} + (L_{mq} + L_f)\frac{di_{eq}}{dt} + L_{mq}\frac{di_{kq}}{dt} \\ U_{kd} = L_{md}\frac{di_d}{dt} + L_{md}\frac{di_{ed}}{dt} + R_{kd}i_{kd} + (L_{md} + L_a)\frac{di_{kd}}{dt} \\ U_{kq} = L_{mq}\frac{di_q}{dt} + L_{mq}\frac{di_{eq}}{dt} + R_{kq}i_{kq} + \left(L_{mq} + L_{kq}\right)\frac{di_{kd}}{dt} \end{array} \right\} \tag{37}$$
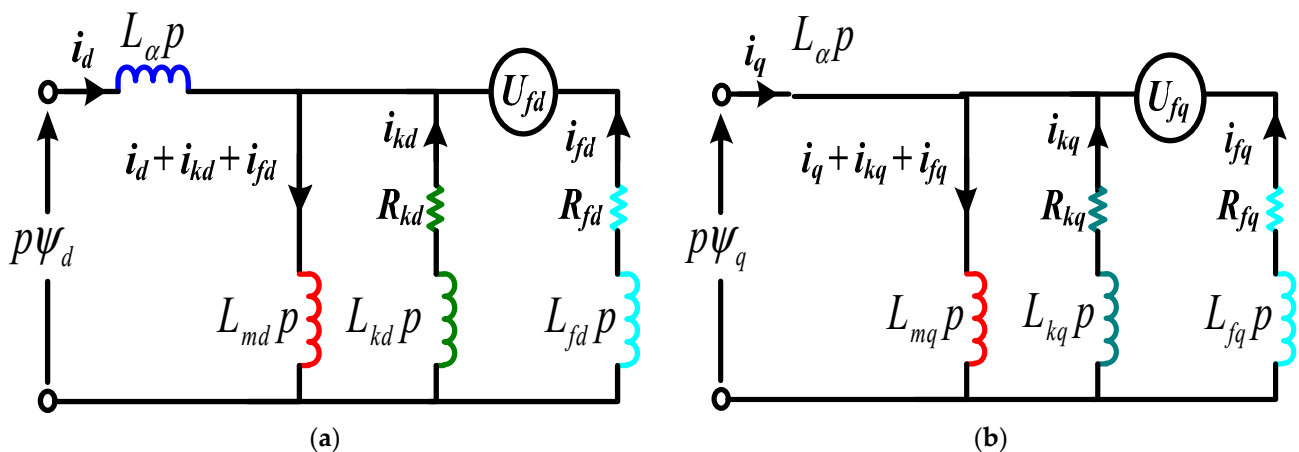
Figure 10. The DESG equivalent circuits: (**a**) direct axis equivalent circuit, and (**b**) quadrature axis equivalent circuit.

6. Experimental Results

The experimental configuration employs a 2.3 kW separately excited DC motor as a turbine emulator, which is mechanically connected to a 2 kW synchronous generator. Within the laboratory setting, a conventional synchronous generator undergoes modifications to become a DESG (doubly excited synchronous generator). This transformation includes the addition of an extra winding and the implementation of the AAR (automatic angle regulator) properly designed to maintain a constant rotor angle, so ensuring system stability. This result is achieved by comparing the output voltage of any phase with a reference signal derived from the rotor. The primary parameters of the DESG employed in the experiments are detailed in Table 3, while additional quantities and parameters associated with the experiments conducted on the DESG can be found in Tables 4–8.

Table 3. Main technical features of the designed DESG prototype.

Parameter	Value
Rated power of the DC motor (Prime Mover)	2.3 KW
Rated power of the DESG	2 KW
Rated voltage	380 V
Rated current	5.6 A
Rated frequency	50 Hz
Number of pair poles	2
Rated speed	1500 rpm
Rated torque	13.369 NM
Efficiency	0.94

Table 4. Parameters of the measured voltage when no load is applied (conventional generator).

$U_{ph}(V)$	I_{an}/ph	$\cos\alpha_n$	E_{on} (V)	θ	P	Q
220	—	—	415	0°	—	—

Table 5. Parameters of the measured voltage with a load applied (conventional generator).

$U_{ph}(V)$	I_{an}/ph	$\cos\alpha_n$	E_{on} (V)	θ_n	P_n (KW)	Q_n(KV)
220	3.55	0.86	415	32°	2	1.15

Table 6. Parameters of the measured voltage with a load applied (provided by the DESG).

| E_{oq}(V)	E_{od}(V)	U_{ph}(V)	I_a/ph	$\cos\alpha_n$	E_{on} (V)	θ_n	P_n (KW)	Q_n(KVAR)
162	385	220	3.55	0.86	415	32°	2	1.15

Table 7. Parameters of the measured voltage with a half load applied to the under test DESG.

E_{oq}(V)	E_{od}(V)	U_{ph}(V)	I_a/ph	$\cos\alpha_n$	E_o (V)	θ	P (KW)	Q (KVAR)
60	309	220	1.75	0.86	315	22°	1	0.575

Table 8. Summary of results related to further different loading conditions for the DESG.

	Capacitive Load (C)	Inductive Load (L)	Resistive Load (R)	Half-Nominal Load (R_{HN-L})	Nominal Load (R_{N-L})
E_o (V)	100	340	308	315	415
E_{oq} (V)	18	21	177	60	162
E_{od} (V)	98	339	253	309	385
V (V)	220	220	220	220	220
P (kW)	0	0.198	2	1	2
Q (kVAR)	−1.15	1.15	0	0.575	1.15
$\theta°$	0	4	45	21	32
$\alpha°$	−87	80	0	30	30
$\delta°$	10	10	10	10	10
$\cos\alpha$	0.05	0.17	1	0.86	0.86

The voltage with no applied load is generated only by means of the direct excitation coil, when the excitation current flows through it ($I_{ed} = I_{edo}$), as shown in Table 4. Figure 11 shows the vector diagram in the no load condition (Figure 11a), and the voltage versus time of the conventional generator with a load angle equal to zero ($\theta = 0°$) (Figure 11b).

(a)   **(b)**
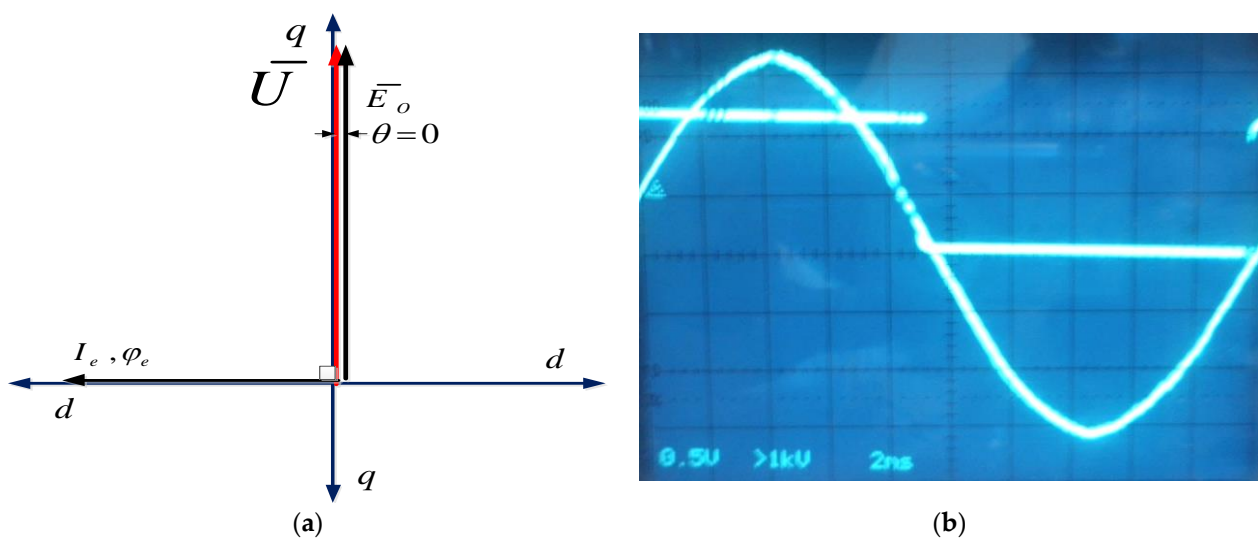
Figure 11. The conventional generator testing with no applied load: (**a**) the vector diagram and (**b**) the generated voltage versus time with a load angle θ equal to zero.

When the conventional generator is connected to a load, specifically U_{ed} = 15 V and I_{ed} = 1.6 A, the obtained results are summarized in Table 5. In this case, the vector diagram
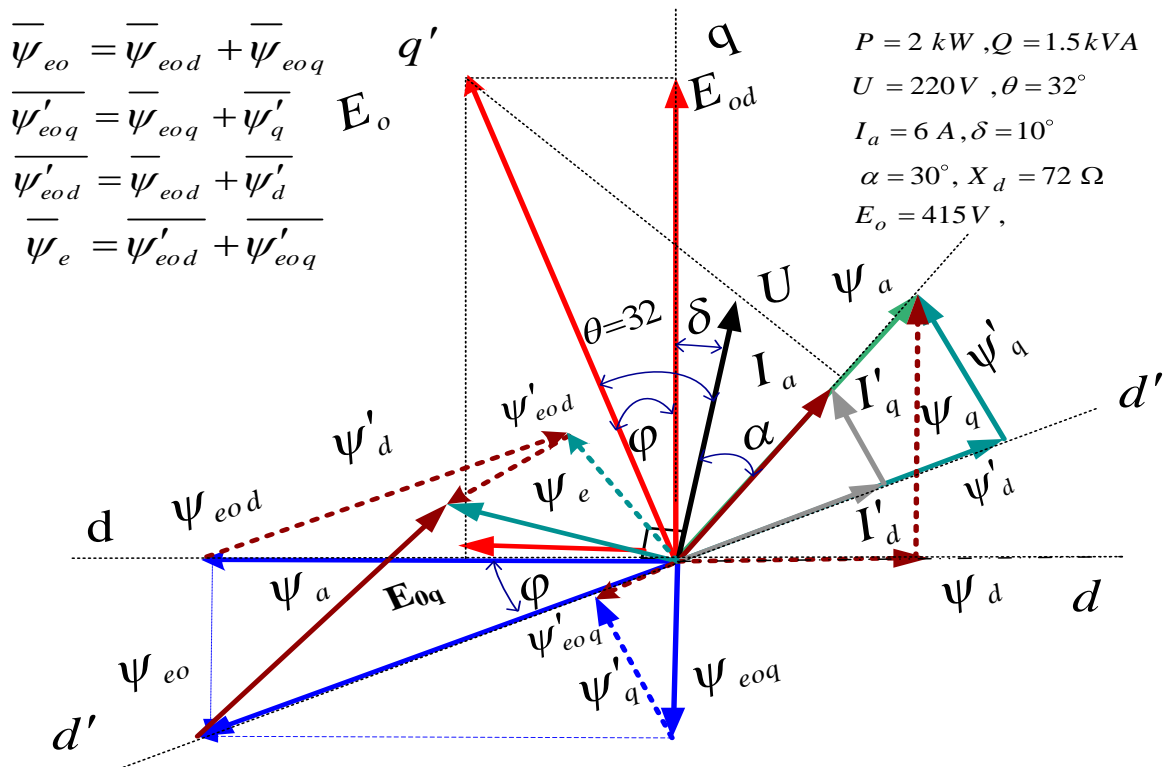
is displayed in Figure 12, while Figure 13 shows the detected voltage versus time of the conventional generator with a load angle θ equal to 32° (matching also with the rotor angle δ).

Figure 12. Vector diagram in the case of a load applied (conventional generator).

Figure 13. For the conventional generator, a plot of the detected voltage versus time with a rotor angle δ (matching with θ) equal to 32°.

As already reported, the laboratory machine is transformed to the DESG by adding an extra winding and using the designed AAR (automatic angle regulator) to keep the rotor angle constant by comparing the output voltage of any phase with a reference signal coming from the rotor. When loading the DESG with a full load, an excitation voltage is applied to the indirect excitation coil (U_{eq}), and then a current I_{eq} flows through it to inject active power into the load. In this way, the rotor angle can be maintained constant, and the sinusoidal wave position of the output voltage (V_a) stays fixed.

For example, the rotor angle δ can be kept constant at 10° by controlling the excitation voltages, U_{eq} and U_{ed}, at 12 V and 9 V, respectively, which induces the currents I_{ed}, equal to 1.2 A, and I_{eq}, equal to 1.8 A. The related parameters of the measured voltage with a load applied are shown in Table 6. According to these results, the vector diagram is represented in Figure 14; furthermore, Figure 15 shows the voltage versus time of the DESG with a rotor angle (δ) equal to 10°, and the load angle (θ) equal to 30°.

$$\overline{\psi}_{eo} = \overline{\psi}_{eod} + \overline{\psi}_{eoq}$$

$$\overline{\psi}'_{eoq} = \overline{\psi}_{eoq} + \overline{\psi}'_{q}$$

$$\overline{\psi}'_{eod} = \overline{\psi}_{eod} + \overline{\psi}'_{d}$$

$$\overline{\psi}_{e} = \overline{\psi}'_{eod} + \overline{\psi}'_{eoq}$$

$$P = 2\,kW,\ Q = 1.5\,kVA$$
$$U = 220\,V,\ \theta = 32°$$
$$I_a = 6\,A,\ \delta = 10°$$
$$\alpha = 30°,\ X_d = 72\,\Omega$$
$$E_o = 415\,V,$$

Figure 14. Vector diagram of the under test DESG with a full load applied.
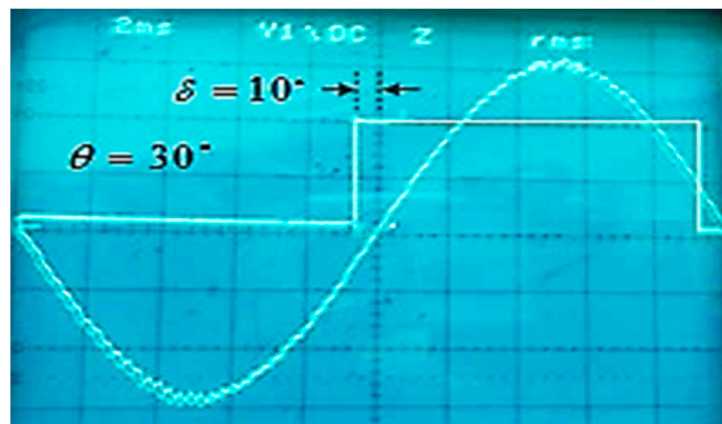
Figure 15. For the under test DESG with a full load applied, the plot of the detected voltage versus time with the rotor highlighted (δ) and load (θ) angles equal to 10° and 30°, respectively.

However, when the DESG is connected to a so-called half load, by applying the excitation values of voltage (U_{ed} = 15 V) and current (I_{ed} = 1.6 A), the obtained results are summarized in Table 7. Figure 16 shows the graphs of voltage versus time, both relating to an applied half load, provided by the conventional generator (rotor angle δ = load angle θ = 22°) (Figure 16a) and by the DESG (rotor angle δ = 10°, load angle θ = 22°). According to these results, the vector diagram is shown in Figure 17. Finally, the obtained experimental results related to further different loading conditions are summarized in Table 8.
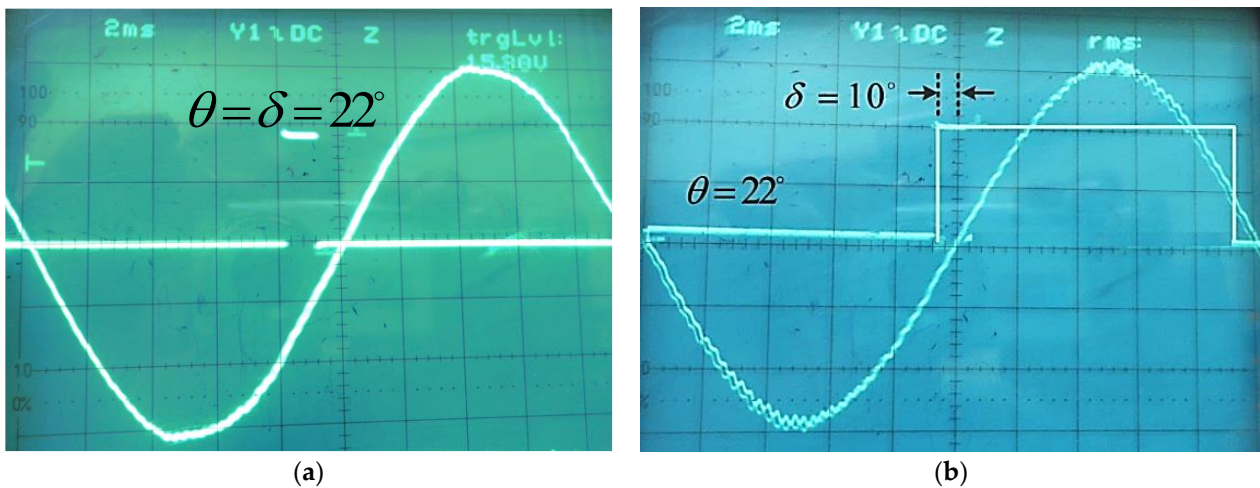
Figure 16. Detected voltage versus time with highlighted rotor δ and load θ angles with a half load applied, as provided by a conventional generator (δ = θ = 22°) (**a**), and by the under test DESG (δ = 10°, θ = 22°) (**b**).
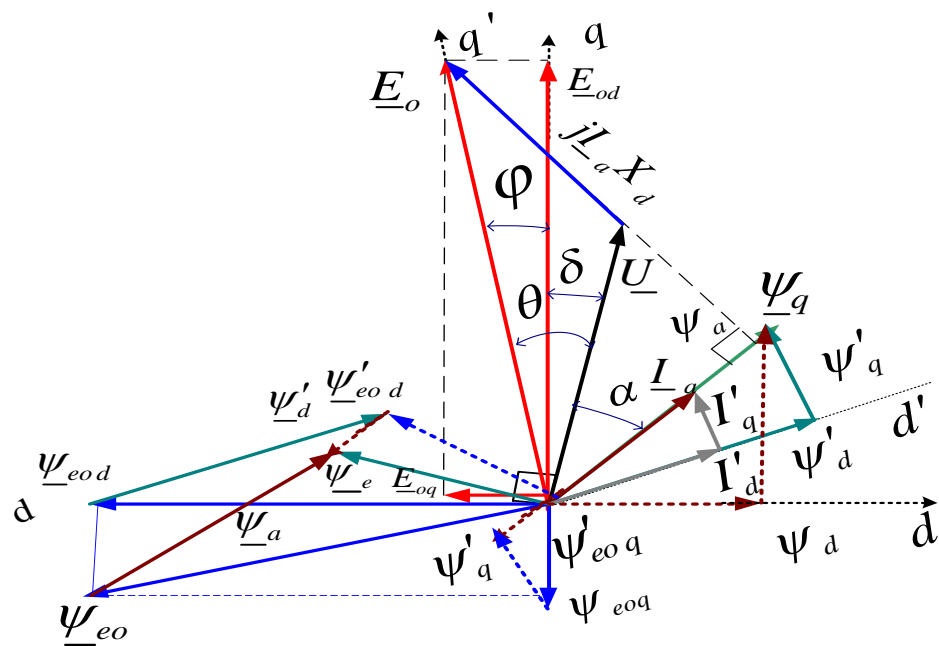

Figure 17. The vector diagram of DESG with a half load applied.

Connection of the DESG to the Grid

In the case of connecting the DESG to the grid, the developed solution is capable of reaching the floating condition by the direct excitation modality. Moreover, the main objective of the quadrature coil is to keep the rotor angle constant under loading so that the system stability can be improved. Therefore, the open voltage is generated by the direct excitation coil after the generator is connected to the grid (in this case, the magnetic flux is not related to the rotor position). Thus, the rotor can take any position according to the excitation current's ratio (I_{ed}/I_{eq}). The load angle θ could be increased to the desired value, increasing the generated active power and decreasing the reactive one. As a result, the power factor will be improved and could reach unity. Thus, the *q*-axis could be known as the power factor improvement axis.

The challenge of rotor angle stability involves investigating the intrinsic electromechanical oscillations within power systems. A key aspect of this issue is how the power outputs of synchronous machines fluctuate with varying rotor angles. Under normal op-

erating conditions, a balance exists between the input mechanical torque and the output electromagnetic torque of each generator, maintaining a constant speed. When the system is disturbed, this equilibrium is lost, leading to the acceleration or deceleration of machine rotors in accordance with the laws of rotating bodies. If a generator temporarily runs at a different speed, its rotor angular position advances relative to the slower machine. The resulting angular difference redistributes some of the load from the slower machine to the faster one, influenced by the strongly nonlinear nature of the power angle relationship. This action reduces the speed disparity and consequently the angular separation. In the case of a conventional synchronous generator, as shown in Figures 12 and 13, the continuous changes in the load angle depend on both the generator's load and the rotor angle. In the case of the DESG, the results obtained in this research work demonstrate that the quadrature coil plays a crucial role in maintaining a constant rotor angle despite load variations, enhancing the rotor angle stability, as shown in Figures 17 and 18.
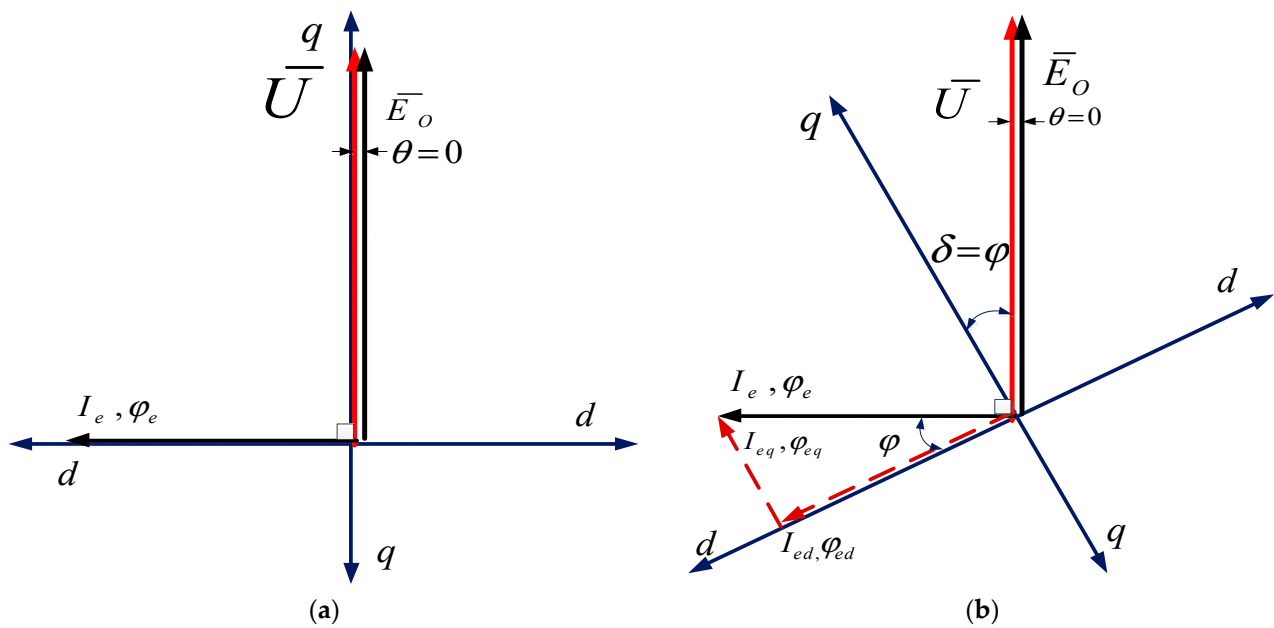
Figure 18. The vector diagram for the floating operation mode referring to the conventional generator ($\theta = \delta = 0$) (**a**), and to the Dual Excitation Synchronous Generator (DESG) ($\theta = 0$, $\delta = \phi$) (**b**).

The following equations represent the floating case when connecting the DESG to the grid (floating condition):

$$P = 0, \ Q = 0, \ I_a = 0, \ \theta = 0 \ \Rightarrow E_0 \cong U \tag{38}$$

$$\theta = (\delta + \varphi) = 0 \ \Rightarrow \delta = -|\varphi| \tag{39}$$

$$E_0 \sin \varphi \cos \delta = E_0 \cos \varphi \sin \delta \ \Rightarrow \ \tan \varphi = \tan \delta \tag{40}$$

$$\Rightarrow \varphi = \delta = \tan^{-1}(I_{eq}/I_{ed}) = \tan^{-1}(E_{oq}/E_{od}); \ U = E_0 \tag{41}$$

Figure 18 shows the vector diagram for the floating operation mode of the conventional generator (Figure 18a) and the DESG (Figure 18b).

The conventional generator or DESG must be connected to the grid by a synchronizer, an electrical arrangement used in the laboratory for successfully synchronizing the electrical machine with the power grid. The electrical connections of the DESG when synchronized to the grid by means of the synchronizer are shown in Figure 19a, according to the electrical diagram realized in the laboratory. Furthermore, the synchronization unit employed in the experimental tests is displayed in Figure 19b, specifically, the model MV 1903 manufactured by the Terco company, Sweden. In Figure 19a, A, B, and C represent the three-phase

terminals of the DESG, CB represents the three-phase circuit breaker, and finally, 1, 2, and 3 correspond to the lamps that appear in Figure 19b, which ensure the success of the synchronization process through a designated light sequence.
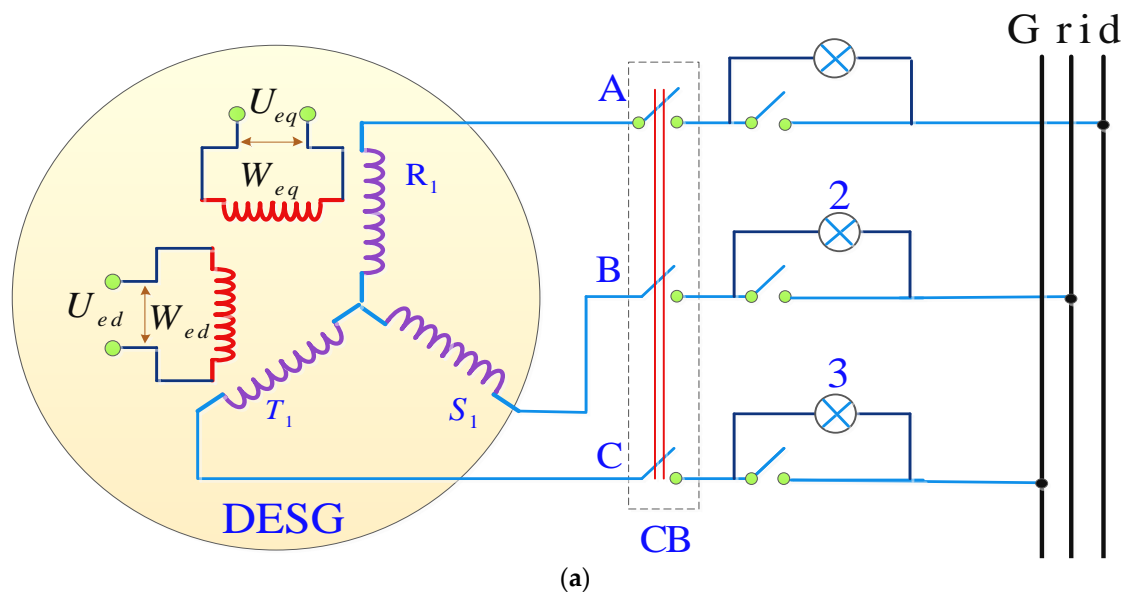

(a)

(b)

Figure 19. The electrical scheme, as realized in the laboratory for the experimental tests, with the DESG connected to the grid through the synchronization unit (**a**); image of the used synchronizing device, model MV 1903 manufactured by Terco company, Sweden (**b**).

Synchronization requires aligning the generator's voltage magnitude, frequency, phase sequence, and phase angle with those of the grid. Failure to comply with these conditions could result in a significant flow of reactive power and potentially harmful mechanical stresses on the generator. The synchronization process can be executed in two different ways: manually or automatically, with the latter being the preferred choice due to its ability to reduce the potential for human error. In the laboratory tests, if the synchronizer's voltmeter indicator dropped to zero, then the phase angle was correct. This result meant that the frequency of the generated voltage was the same as the grid; therefore, the synchronous generator was synchronized with the grid.

The grid voltage was characterized by a 218 V amplitude with a frequency of 49.4 Hz. When the electric machine was in floating mode, the excitation voltage and current were $U_{exd} = 14.7$ V and $I_{exd} = 1.4$ A, respectively. However, when the generator injected a power P equal to 525 W (voltage and current values U = 220 V and I_a = 2.4 A, respectively),

the main excitation voltage was maintained constant, as well as the excitation current; this is because the power injection was performed by increasing the torque applied to the machine.

It is noted from Figure 20a that the temporal trend of the voltage is shifted from the reference pulse by an 18° angle, namely the load angle, and it is equal to the calculated value. This result is obtained without using the quadrature winding. While, by using the quadrature excitation with the regulator AAR at the same power, the excitation voltage and current on the *q*-axis were U_{exq} = 6 V and I_{exq} = 0.38 A, respectively, and the excitation voltage and current on the *q*-axis became U_{exd} = 13.4 V and I_{exd} =1.35 A, respectively. As a result, the rotor angle δ was kept constant at the value of 10°, as shown in Figure 20b.
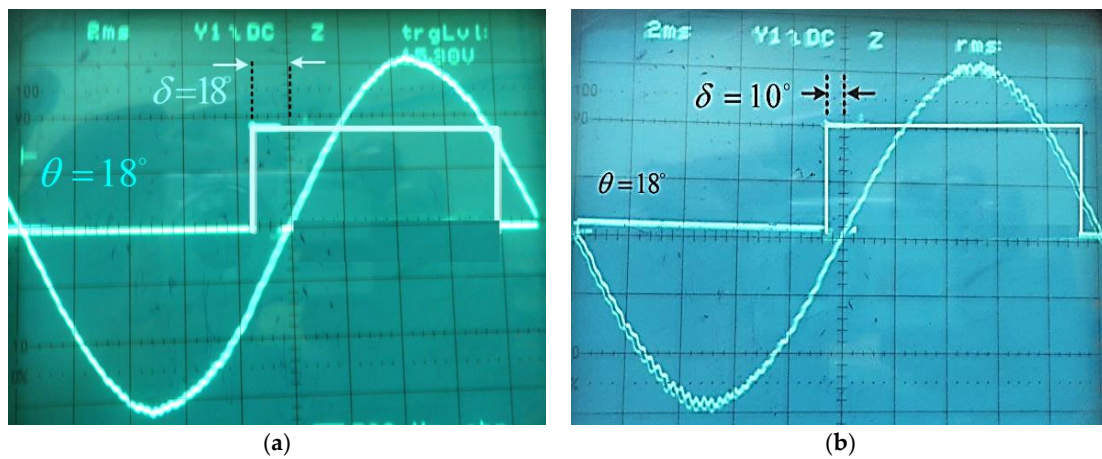
Figure 20. Voltage trend over time for the (**a**) conventional generator (rotor angle δ = load angle θ = 18°), and (**b**) DESG (rotor angle δ equal to 10°, load angle θ equal to 18).

The following vector diagram illustrates how the power P and Q increase with increasing E. In many cases, the changes in P and Q depend on E_o by the amount of $\pm\Delta E$, as shown in Figure 21.
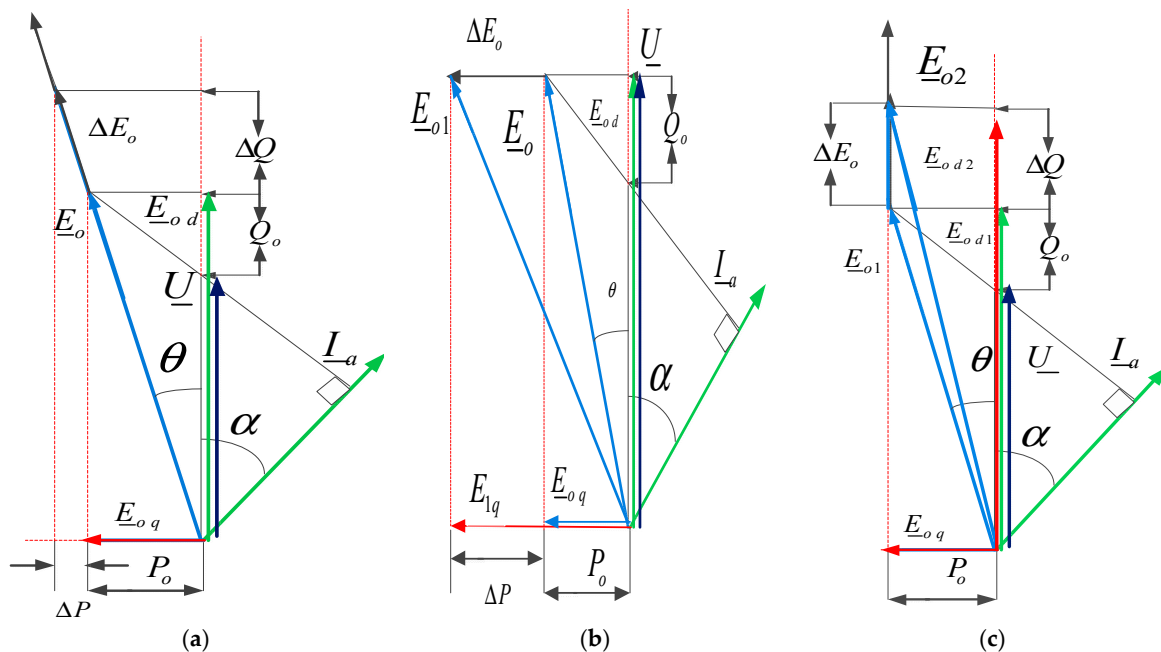

Figure 21. The variation of P and Q: (**a**) ΔE_o increase in the direction of E_o, $\Rightarrow \Delta P$, ΔQ increase, (**b**) ΔE_o increase perpendicularly on U $\Rightarrow \Delta P$ increase only, (**c**) ΔE_o increases in parallel with the U $\Rightarrow \Delta Q$ increase only.

7. Results Discussion

Referring to the vector diagrams for all the loading cases (Figure 21), we can observe that the magnitude and angle of the flux ϕ_e remained constant, regardless of the loading angle. This result is due to the presence of the quadrature winding, which generates the magnetic flux compensating for the actual flux of the armature reaction. Thus, the load angle can be changed and the generated power will change accordingly, keeping the rotor angle δ constant; this operation can be executed by controlling the angle ϕ (by using the following relations $\tan\phi = E_q/E_d$ and $\theta = \phi + \delta$). Consequently, the stability angle ϕ is independent of the load angle.

Equation (3) represents the relationship of the active power in the DESG as a function of the rotor angle (δ). As the value of δ is small, the first component of this equation is negligible, while the second component is the most significant. Hence, almost all the power generated is obtained from the second term, which represents the power delivered on the *q*-axis, obtaining the following expression:

$$P = mUK_{iq}I_{eq} \tag{42}$$

The same considerations can be applied to Equation (4):

$$Q = mUK_{id}I_{ed} \ - \ mU^2/X_d \tag{43}$$

Any change in the generated reactive power is regulated by the excitation current I_{ed} of the longitudinal direct winding, or simply the reactive power winding, in which the reactive power can be controlled for leading and lagging any loads. The variation of the P and Q depends on E_o through the amount of $\pm\Delta E$. In the DESG machines, the value of E_o can be changed by changing E_q or E_d, e.g., by increasing E_q, E_o will be increased perpendicularly to the U direction, and the generated active power P increases as well. Conversely, when E_d is changed, E_o will be changed in the direction parallel to the voltage U direction, and the generated reactive power Q increases. During normal operating conditions, the variation of E_o is in an undefined direction, and P and Q vary simultaneously. Thus, the other excitation winding provides the generator with greater flexibility to regulate and control the active and reactive power separately. When the generator is connected to the network, the developed solution is capable of keeping the rotor angle fixed, whatever the actual injected power, by controlling the excitation voltage of the perpendicular winding. The main disadvantage of DESG is the increased cost due to the automatic control system necessary.

In summary, the approach adopted in this paper relies on laboratory experiments. The conventional synchronous generator underwent modification by introducing an additional excitation winding along the *q*-axis, perpendicular to the conventional excitation winding along the *d*-axis, enabling control over both active and reactive power. Two orthogonal excitation coils, *d* and *q*, were created from the existing coils, and the experimental tests were conducted across all loads with a fixed rotor angle (i.e., stability angle φ). The research study utilized two laboratory models: The first involves a 2 kW capacity DESG driven by a DC motor simulating a wind turbine. The mechanical coupling proposed in the paper was implemented in this experimental setup between the two machines. The second model is a three-phase laboratory machine with a nominal capacity of 2.3 KVA. Experimental tests were conducted on all loads using a three-phase synchronous generator driven by a DC motor, and mathematical equations were derived to develop a mathematical model. The paper investigated and compared the performance of the DESG with a conventional synchronous generator. The experimental findings affirm that the DESG enhances the generator stability significantly by maintaining a constant rotor angle δ. The developed solution necessitates the use of an automatic angle regulator (AAR) in addition to the conventional automatic voltage regulator (AVR).

The key findings obtained throughout the research work are as follows:

1. Developing two laboratory models: The first is a synchronous generator with a 2 kW capacity, specifically a double excitation cylindrical generator, where the electrical

circuit was rewound to form two excitation coils. This generator was driven by a DC motor representing the wind turbine, with the generator and motor linked through the mechanical coupling developed in this research. The second model is a three-phase laboratory machine with a nominal capacity of 2.3 KVA. Two perpendicular excitation coils, d and q, were formed from the existing coils, and tests were carried out on all loads, ensuring that the revolving angle (namely the stability angle ϕ) was fixed.

2. It has been proven that it is possible to modify the load angle and adjust the generator capacity accordingly while ensuring the rotor angle (δ) constant. This means that the stability angle ϕ is decoupled from the load and, consequently, from the generated power. The generator consistently maintains its rotation at the designated synchronous speed, unaffected by the employed load. In other words, both the rotational speed and frequency remain unchanged regardless of the generator's load.

3. Upon connection to the grid, it is possible to maintain a constant rotor angle, regardless of the injected power, by regulating the excitation voltage applied to the cross-excitation coil.

4. It is now feasible to independently control both the real and reactive power (for the latter, relating to both types of loads, capacitive or inductive), independently. Additionally, the regulation of the power factor (and its consequent improvement) has become achievable.

5. The manuscript provides a complete description of the electrical generators discussed and all the mathematical relationships and performance curves, which have also been validated through experimental testing. Furthermore, to further highlight the results presented and the scientific value of the research work, keep in mind that most of the published research on dual excitation generators is primarily theoretical and lacks support from laboratory experimentation.

6. The potential to employ the suggested innovative approach for directly connecting the wind turbine-driven synchronous generator to the grid is noteworthy. This innovative solution would eliminate the need for additional electronic components and reduce the occurrence of malfunctions during prolonged and uninterrupted operations.

7. Implementing this method could result in substantial cost reductions, potentially reaching 15–20% of the generator's overall price. These savings stem from the adoption of the designed mechanical coupling, which replaces the conventional use of inverters for frequency correction. The estimated cost of the electronics replaced by the innovative mechanical coupling accounts for approximately 15–20% of the total cost.

8. Conclusions

It is important to mention that the primary drawback of the presented solution is the rise in expenses associated with the automatic control system. In exchange, numerous benefits have been achieved, among which, above all, is the enhancement of the static and dynamic stability coefficients, particularly under lighter and capacitive loads, and a high level of reliability in delivering the necessary power across various operating conditions. Furthermore, the direct connection of the synchronous generator to the grid was achieved without the need for any power components or converters. This connecting method ensures a consistent generator output voltage, maintains a constant frequency aligned with the network frequency, and guarantees a pure sine wave output voltage. When applied to wind turbines, these characteristics remain unaffected by changing wind speed. The described mechanism was successfully implemented for both DESG and conventional synchronous generators, as detailed in the manuscript. When applied to the wind generator, the proposed technique allows for avoiding the integration of a power converter for transferring power into the power grid, thus improving the system's reliability. The only drawback of the proposed method is the need for an automatic control system to modulate the signals on the quadrature coils and manage the power transfer into the electrical network.

As future steps of the proposed solution, we will test the developed control strategy in a real scenario, that is, in a medium-sized wind generation system with a low kilowatt power output, validating its capability to independently control both the real and reactive power under changing grid parameters over time. In more detailed future research, our aim will be to determine the technical performance of the developed solution employed in a real application, taking into account the variability of the wind and the operating conditions, and to exactly evaluate with the wind plant's managers the advantages of the proposed solution, also in economic terms, compared to the standard solutions implemented so far for connection to the electricity distribution network.

References

1.   Huang, J.; Tu, G.; Chen, D. Nonlinear Optimal Excitation Control of Dual-Excited Synchronous Generators. *IFAC Proc. Vol.* **1997**, *30*, 69–74. [CrossRef]
2.   Morsy, M.S.; Amer, H.H.; Badr, M.A.; El-Serafi, A.M. Transient Stability of Synchronous Generators with Two Axis Slip Frequency Excitation. *IEEE Trans. Power Appar. Syst.* **1983**, *PAS-102*, 852–1004. [CrossRef]
3.   Hayashi, S.; Haraguchi, E.; Sanematsu, T.; Takahashi, N.; Yasaka, Y.; Nogura, O. Development of Adjustable Speed Generator. In Proceedings of the International Conference on Large High Voltage Electric Systems (CIGRE), Paris, France, 28 August–3 September 1988. Paper n. 11-03.
4.   Yassin, H.M.; Abdel-Wahab, R.R.; Hanafy, H.H. Active and Reactive Power Control for Dual Excited Synchronous Generator in Wind Applications. *IEEE Access* **2022**, *10*, 29172–29182. [CrossRef]
5.   Yonah, Z.O.; El-Serafi, A.M.; Krause, A.E. Performance of a Computer-Based Two-Phase Excitation System for a Variable-Speed Dual-Excited Synchronous Generator. In Proceedings of the WESCANEX Conference on Communications, Computers and Power in the Modern Environment, Saskatoon, SK, Canada, 17–18 May 1993; pp. 263–268. [CrossRef]
6.   Reddy, A.A.; Bhat, S.S. Modeling of Dual Excited Synchronous Generator with slip frequency excitation. In Proceedings of the 2020 IEEE First International Conference on Smart Technologies for Power, Energy and Control (STPEC), Nagpur, India, 25–26 September 2020. [CrossRef]
7.   Yonah, Z.O.; El-Serafi, A.M.; Krause, A.E. Regulation of terminal voltage and output frequency of a variable speed dual-excited synchronous generator by using a computer-based two-phase excitation system. In Proceedings of the Canadian Conference on Electrical and Computer Engineering, Vancouver, BC, Canada, 14–17 September 1993; pp. 1165–1168. [CrossRef]
8.   Lipo, T.A. *Analysis of Synchronous Machines*, 2nd ed.; CRC Press: Boca Raton, FL, USA, 2012; ISBN 978-1138073074.
9.   Fraihat, H.; Almbaideen, A.A.; Al-Odienat, A.; Al-Naami, B.; De Fazio, R.; Visconti, P. Solar Radiation Forecasting by Pearson Correlation Using LSTM Neural Network and ANFIS Method: Application in the West-Central Jordan. *Future Internet* **2022**, *14*, 79. [CrossRef]
10. Adkins, B.; Harley, R.G. *The General Theory of Alternating Current Machines: Application to Practical Problems*; Springer: Dordrecht, The Netherlands, 1975; ISBN 978-94-009-5802-9. [CrossRef]
11. Anderson, P.M.; Fouad, A.A. *Power System Control and Stability*; Wiley-IEEE Press: New York, NY, USA, 1995; Chapters 1–28; 672p, Available online: https://ieeexplore.ieee.org/servlet/opac?bknumber=5264012 (accessed on 28 August 2023).
12. Yassin, H.M.; Abdel Wahab, R.R.; Hanafy, H.H. Investigation of LVRT Capability of Wind Driven Dual Excited Synchronous Generator. *Wind. Eng.* **2023**, *47*, 369–384. [CrossRef]
13. Abdel-Wahab, R.R.; Yassin, H.M.; Hanafy, H.H. Dual Excited Synchronous Generator a Suitable Alternative for Wind Applications. In Proceedings of the 2020 IEEE 14th International Conference on Compatibility, Power Electronics and Power Engineering (CPE-POWERENG), Setubal, Portugal, 8–10 July 2020; Volume 1, pp. 352–357.

14. D'Arco, S.; Piegari, L.; Tricoli, P. A Novel Control of Dual-Excited Synchronous Machines for Variable-Speed Wind Turbines. In Proceedings of the 2011 IEEE Trondheim PowerTech, Algiers, Algeria, 19–23 June 2011; pp. 1–6.
15. Dekali, Z.; Baghli, L.; Boumediene, A. Indirect Power Control for a Grid Connected Double Fed Induction Generator Based Wind Turbine Emulator. In Proceedings of the 2019 International Conference on Advanced Electrical Engineering (ICAEE), Algiers, Algeria, 19–21 November 2019; pp. 1–6.
16. Bruck, R.W.; Messerle, H.K. The capability of alternators. *Proc. Inst. Electr. Eng.* **1955**, *102 Pt A*, 645–647. [CrossRef]
17. Kosow, I.L. *Electrical Machinery and Transformer*, 2nd ed.; Prentice Hall: Hoboken, NJ, USA, 2009; ISBN 9780132487337.
18. El-Hawary, M.E. *Principles of Electrical Machine with Power Electronic Applications*, 2nd ed.; Wiley-IEEE Press: Hoboken, NJ, USA, 2002; Available online: https://ieeexplore.ieee.org/servlet/opac?bknumber=5264263 (accessed on 29 August 2023).
19. Richardson, D.V.; Caisse, A.J. *Rotating Electric Machinery and Transformers Technology, Pearson*, 4th ed.; Pearson: London, UK, 1996; ISBN -13-978-0134096407.
20. Nasar, S.A. *Electric Machines and Power Systems: Volume I, Electric Machines*; McGraw Hill: New York, NY, USA, 1995; ISBN -13-978-0070459588.
21. Sarma, M.S. *Electric Machines: Steady—State Theory and Dynamic Performance*; Cengage Learning: Boston, MA, USA, 1997; ISBN -13-978-0534938437.
22. Krause, P.C.; Towle, J.N. Synchronous machine damping by excitation control with direct and quadrature axis field windings. *IEEE Trans. Power Appar. Syst.* **1969**, *88*, 1266–1274. [CrossRef]
23. Xu, G.; Hu, Y.; Hao, X.; Zhan, Y.; Zhao, H.; Liu, X.; Luo, Y. The relationship of magnetomotive force under different excitation modes of dual-excited synchronous generator. *IEEE Trans. Magn.* **2018**, *54*, 8200704. [CrossRef]
24. Bidadfar, A.; Nee, H.-P.; Zhang, L.; Harnefors, L.; Namayantavana, S.; Abedi, M.; Karrari, M.; Gharehpetian, G.B. Power system stability analysis using feedback control system modelling including HVDC transmission links. *IEEE Trans. Power Syst.* **2016**, *31*, 116–124. [CrossRef]
25. Kapoor, S.C.; Kalsi, S.S.; Adkins, B. Improvement of alternator stability by controlled quadrature excitation. *Proc. Inst. Electr. Eng.* **1969**, *116*, 771–780. [CrossRef]
26. Vitale, A.; Stoyka, K.; Venere, E.; Visconti, P. Design and Optimization of a Post-Regulated Inductive Power Transfer System with a Series-Series Compensation. In Proceedings of the 14th International Conference of the International Association for Mathematics and Computer in Simulation—Electrimacs, Nancy, France, 16–22 May 2022; Lecture Notes in Electrical Engineering. Springer: Cham, Switzerland, 2023; Volume 993, pp. 209–223. [CrossRef]
27. Stoyka, K.; Vitale, A.; Venere, E.; Visconti, P. Enhanced Static and Dynamic Modeling of a Series-Series Inductive Power Transfer System with a Buck Post-Regulator. In Proceedings of the 14th International Conference of the International Association for Mathematics and Computer in Simulation—Electrimacs, Nancy, France, 16–22 May 2022; Lecture Notes in Electrical Engineering. Springer: Cham, Switzerland, 2023; Volume 993, pp. 193–207. [CrossRef]
28. Yousefian, R.; Bhattarai, R.; Kamalasdan, S. Transient stability enhancement of power grid with integrated wide-area control of wind farms and synchronous generators. *IEEE Trans. Power Syst.* **2017**, *32*, 4818–4831. [CrossRef]
29. Ong, C.-M. *Dynamic Simulation of Electric Machinery Using Matlab/Simulink*; Prentice Hall PTR: Hoboken, NJ, USA, 1998; ISBN -13-978-0-13-723785-2.